

# On Equivariant Model Selection through the Lens of Uncertainty

Putri A. van der Linden<sup>\*,1</sup>Alexander Timans<sup>1,2</sup>Dharmesh Tailor<sup>1</sup>Erik J. Bekkers<sup>1</sup><sup>1</sup>Amsterdam Machine Learning Lab, University of Amsterdam<sup>2</sup>UvA-Bosch Delta Lab, University of Amsterdam

## Abstract

Equivariant models leverage prior knowledge on symmetries to improve predictive performance, but misspecified architectural constraints can harm it instead. While work has explored learning or relaxing constraints, selecting among pretrained models with varying symmetry biases remains challenging. We examine this model selection task from an uncertainty-aware perspective, comparing frequentist (via Conformal Prediction), Bayesian (via the marginal likelihood), and calibration-based measures to naive error-based evaluation. We find that uncertainty metrics generally align with predictive performance, but Bayesian model evidence does so inconsistently. We attribute this to a mismatch in Bayesian and geometric notions of model complexity, and discuss possible remedies. Our findings point towards the potential of uncertainty in guiding symmetry-aware model selection.

## 1 INTRODUCTION

Real-world tasks frequently exhibit geometric symmetries such as rotations or reflections, and equivariant predictive models for such settings have proven effective on problems ranging from medical imaging [Fu et al., 2023] to molecule synthesis [Atz et al., 2021, Batzner et al., 2022] and physics simulations [Brandstetter et al., 2021]. Such geometric knowledge is generally embedded as constraints on model expressivity, and misspecifying the inductive bias may harm performance [Petrache and Trivedi, 2023]. This has led to recent work on *learning* equivariance and softening constraints, e.g. Romero and Lohit [2022], Moskalev et al. [2023], van der Linden et al. [2024], including from a Bayesian model selection perspective [van der Wilk et al., 2018, van der Ouderaa et al., 2023]. Yet such relaxations

also remain architecturally tied, and from a practitioner’s *post-hoc* perspective it remains unclear what model to favor when faced with a range of pretrained options, from fully unconstrained to strictly equivariant. While a simple hold-out error comparison (e.g. on accuracy) is possible, measures that incorporate notions of *uncertainty* have been advocated for more robust model assessment [Begoli et al., 2019, Makridakis and Bakas, 2016], resulting in much work on uncertainty for neural networks [Gawlikowski et al., 2023].

Taking this perspective, we investigate equivariant model selection through the lens of uncertainty. Given differently constrained architectures, we verify how *post-hoc* frequentist (via Conformal Prediction intervals), Bayesian (via the marginal likelihood) and calibration measures compare to a simple error-based evaluation. Our experiments on object shapes (ModelNet40) and molecule data (QM9) suggest that uncertainty-based model recommendations generally align with predictive error, but the Bayesian model selection framework does so inconsistently. We posit that this results from misaligned notions of Bayesian and geometric model complexity in the marginal likelihood, and discuss perspectives on addressing this interesting and challenging problem. Our findings suggest the potential of uncertainty-aware frameworks in guiding equivariant model selection.

## 2 BACKGROUND

We next provide some brief background on equivariance and uncertainty-related topics relevant for this work.

**Equivariance and invariance.** A map  $f : \mathcal{X} \rightarrow \mathcal{Y}$  is said to be *invariant* to a given transformation group  $G$  if it satisfies the condition

$$f(\mathbf{x}) = f(g \circ \mathbf{x}) \quad \forall g \in G, \quad (1)$$

where we loosely use  $\circ$  as the application of transformation  $g$ <sup>1</sup>. This property implies the output of a function is left

<sup>1</sup>Formally, a group element  $g$  acts on a space via the group action  $\rho(g)$ . See Bronstein et al. [2021] for a thorough treatment.

\*Corresponding author: p.a.vanderlinden@uva.nl

unchanged when the input is transformed by  $G$ . Similarly, a function is said to be *equivariant* if it satisfies

$$g \circ f(\mathbf{x}) = f(g \circ \mathbf{x}) \quad \forall g \in G, \quad (2)$$

meaning that the output transforms in a structured, predictable way under the action of  $G$ . While equivariance preserves geometric structure through the transformation, invariance discards it. These properties are usually enforced through architectural constraints that ensure transformation-preserving layers, e.g. Cohen and Welling [2016], Weiler and Cesa [2019]. However, invariance can also be approximately enforced via *data augmentation* during training, encouraging the model to produce identical outputs for transformed inputs [Lyle et al., 2020].

**Conformal prediction and calibration.** *Conformal prediction* offers a popular framework to extend a model’s pointwise predictions to prediction set estimation. The approach is fully data-driven, *post-hoc*, and amenable to both classification and regression [Fontana et al., 2023]. Crucially, relying on a data exchangeability argument (*i.e.* relaxed *i.i.d.*’ness) a probabilistic coverage guarantee for unseen test samples can be provided, attaching a notion of reliability to obtained uncertainties [Shafer and Vovk, 2008]. In contrast, probabilistic *calibration* does not provide explicit guarantees, but instead captures a notion of asymptotic consistency between predicted and observed outcomes [Guo et al., 2017, Silva Filho et al., 2023]. That is, whether a model’s prediction confidence  $\hat{p}$  aligns with the target’s true observed frequency  $p$  in the data, rendering it trustworthy.

**Bayesian model selection.** Within a Bayesian context, a model  $\mathcal{M}$ ’s ability to explain observed data  $\mathcal{D}$  can be evaluated via the *marginal likelihood*, formally denoted as

$$p(\mathcal{D}|\mathcal{M}) = \int p(\mathcal{D}|\boldsymbol{\theta}, \mathcal{M}) p(\boldsymbol{\theta}|\mathcal{M}) d\boldsymbol{\theta}. \quad (3)$$

Also referred to as *model evidence*, the quantity averages the data likelihood  $p(\mathcal{D}|\boldsymbol{\theta}, \mathcal{M})$  over the prior  $p(\boldsymbol{\theta}|\mathcal{M})$  for model parameters  $\boldsymbol{\theta}$ , effectively quantifying data fit while penalizing overly complex models that assign low prior probability to regions of high likelihood [MacKay, 2003]. This naturally integrates *Occam’s Razor* as a model selection principle, where the model with highest  $p(\mathcal{D}|\mathcal{M})$  is preferred [Rasmussen and Ghahramani, 2000] and arguably generalizes more favourably [Germain et al., 2016, Lotfi et al., 2022]. As Eq. 3 is generally intractable, and in particular for large-scale neural networks, efficient and scalable approximations become necessary [Llorente et al., 2023].

### 3 UNCERTAINTY MEASURES FOR MODEL SELECTION

We next detail the particular uncertainty-based measures we employ based on the above frameworks to assess model fit.

**Conformal prediction set size.** The satisfaction of conformal coverage guarantees at some target level  $1-\alpha$  (e.g. 90%) is met by design, thus we focus on assessing model fit by the *efficiency* of obtained prediction sets, where smaller set size indicates more informative uncertainty [Shafer and Vovk, 2008]. Given test observations  $(\mathbf{x}_i, \mathbf{y}_i) \in \mathcal{D}_{test}$  and produced prediction sets  $C(\mathbf{x}_i)$ , the *mean set size* is simply

$$\text{Mean set size} = \frac{1}{|\mathcal{D}_{test}|} \sum_{i \in \mathcal{D}_{test}} |C(\mathbf{x}_i)|. \quad (4)$$

We combine the models outlined in § 4 with simple top-class and residual scoring to construct the conformal prediction sets (see Appendix B), and refer to Angelopoulos et al. [2023] for an introductory work covering these mechanisms.

**Calibration error.** For classification, the *expected calibration error* (ECE) is commonly employed despite some pathologies [Guo et al., 2017, Nixon et al., 2019]. Therein confidence levels are binned and the gap to similarly binned model accuracies is measured, thus favouring a smaller ECE that better aligns model confidence and output. We additionally measure the *Brier score* [Brier, 1950], a classical probabilistic scoring rule whose decomposition expresses both calibration and efficiency properties of the model [Gneiting et al., 2007, Murphy, 1973]. For regression tasks the notion of calibration is ambiguously defined, but tends to pertain to coverage properties of estimated intervals [Kompa et al., 2021, Kuleshov et al., 2018]. In that context, conformal prediction intervals can also be framed as a calibration procedure [Dheur and Taieb, 2023], and we do not consider any additional measures.

**Bayesian model selection via the Laplace approximation.** We employ Laplace’s method [MacKay, 1992] to obtain a tractable approximation of Eq. 3. Therein, a second-order Taylor expansion for the unnormalized log-posterior  $p(\boldsymbol{\theta}|\mathcal{D}, \mathcal{M})$  around a local optimum  $\boldsymbol{\theta}_*$  (here, the pretrained model’s weights) yields the distinct terms

$$\begin{aligned} \log p(\mathcal{D}|\mathcal{M}) \approx & \underbrace{\log p(\mathcal{D}|\boldsymbol{\theta}_*, \mathcal{M})}_{\text{Data fit}} \\ & - \underbrace{\left[ \frac{1}{2} \log \left| \frac{1}{2\pi} \mathbf{H}_* \right| - \log p(\boldsymbol{\theta}_*|\mathcal{M}) \right]}_{\text{Model complexity}}, \end{aligned} \quad (5)$$

where  $\mathbf{H}_* = -\nabla_{\boldsymbol{\theta}}^2 \log p(\mathcal{D}|\boldsymbol{\theta}_*, \mathcal{M}) + \delta \mathbf{I}$  is the Hessian of the negative log likelihood and  $\delta$  is the precision of the isotropic Gaussian prior  $p(\boldsymbol{\theta}|\mathcal{M}) = \mathcal{N}(\mathbf{0}, \delta^{-1} \mathbf{I})$ . The trade-off between data fit (the log-likelihood evaluated at  $\boldsymbol{\theta}_*$ ) and model complexity in the Bayesian sense becomes apparent. As we aim for *post-hoc* model selection, we follow the recommendation of Daxberger et al. [2021] for a *last-layer* Laplace approximation<sup>2</sup>, wherein  $\mathbf{H}_*$  is computed only over the last linear model layer. Other approximations such as KFAC or diagonal are also possible [Immer et al., 2021].

<sup>2</sup>Using <https://aleximmer.com/Laplace/>

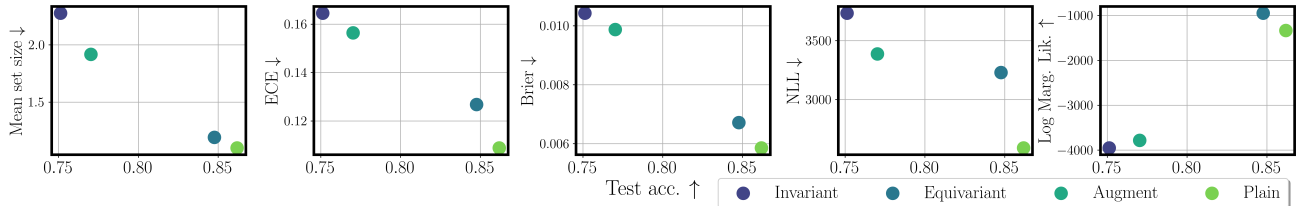


Figure 1: We visualize alignment between uncertainty-based measures (y-axis) and prediction accuracy (x-axis) on ModelNet40 test data for all four models (§ 4). ‘NLL’ refers to the *negative log-likelihood* of the model’s direct softmax output (*i.e.* not using Laplace), while ‘Log Marg Lik’ equates Eq. 5. (↑↓) indicate the desired direction of the measure.

Target	Model $\mathcal{M}$	Train data $\mathcal{D}_{train}$				Test data $\mathcal{D}_{test}$	
		MAE ↓	LogLik ↑	Complexity ↓	Log-MargLik ↑	MAE ↓	LogLik ↑
$\mu$	Invariant	0.0025	-101084	767	-101851	0.0204	22064
	Equivariant	0.0083	-101091	723	<b>-101814</b>	<b>0.0145</b>	<b>22940</b>
	Augment	0.0048	-101086	799	-101886	0.0254	20826
	Plain	0.0038	-101086	798	-101884	0.0296	19622
$\alpha$	Invariant	0.0102	-101097	1530	<b>-102628</b>	0.0613	768
	Equivariant	0.0290	-101176	1515	-102691	<b>0.0522</b>	<b>9014</b>
	Augment	0.0153	-101112	1521	-102633	0.0679	-3732
	Plain	0.0106	-101100	1564	-102664	0.0888	-19273
$\varepsilon_{HOMO}$	Invariant	0.2540	-101083	1211	-102295	23.4848	20586
	Equivariant	2.9681	-101084	1243	-102327	<b>21.3705</b>	<b>20989</b>
	Augment	0.7900	-101083	1149	-102233	27.4825	19461
	Plain	0.2288	-101083	1148	<b>-102231</b>	33.6994	17578
$\varepsilon_{LUMO}$	Invariant	0.9781	-101083	416	-101500	20.2211	21650
	Equivariant	4.3102	-101085	465	-101550	<b>19.3362</b>	<b>22028</b>
	Augment	1.3789	-101083	414	-101498	21.6268	21417
	Plain	1.0273	-101083	361	<b>-101445</b>	24.2827	20628
$C_v$	Invariant	0.0134	-101112	1345	-102457	0.0298	19330
	Equivariant	0.0180	-101121	1326	-102447	<b>0.0275</b>	<b>20017</b>
	Augment	0.0107	-101104	1334	<b>-102438</b>	0.0331	18098
	Plain	0.0066	-101094	1357	-102451	0.0394	15812

Table 1: We tabularize results for all four models (§ 4) and five regression targets on QM9 train and test data. We report predictive error (via the *mean absolute error*, MAE) and the Laplace-based terms in Eq. 5: data fit via the log-likelihood (LogLik), Bayesian model complexity, and the overall log-marginal likelihood (Log-MargLik). (↑↓) indicate the desired direction of the measure, and we highlight the **preferred model** according to different selection criteria.

## 4 EXPERIMENTAL RESULTS

We next outline our experimental design and results, and defer further implementation details to Appendix B. We consider two prediction tasks and datasets: classification on ModelNet40 [Wu et al., 2015] and regression on QM9 [Ramakrishnan et al., 2014]. ModelNet40 consists of  $\sim 12\,000$  rotationally aligned objects across 40 classes and hence does *not* strictly require  $SO(3)$  invariance. QM9 contains  $\sim 130\,000$  molecular point clouds with several scalar targets, of which we consider  $\mu$ ,  $\alpha$ ,  $\varepsilon_{HOMO}$ ,  $\varepsilon_{LUMO}$  and  $C_v$  (separate models are trained for each target). Due to arbitrary molecular orientations, invariance to the  $SO(3)$  group is generally considered necessary here.

**Model choice.** We evaluate four variations of the message-passing architecture PONITA [Bekkers et al., 2024], which are implemented in Vadgama et al. [2025] as Rapidash.

The Rapidash model is well-suited for our study as it enables explicit control over the equivariance constraints employed within layers, and else maintains the same architecture. We consider the following choices:

1. **Invariant:** constrained via invariant message passing layers;
2. **Equivariant:** constrained via equivariant message passing layers;
3. **Augment:** same as **Plain** but trained with  $SO(3)$  data augmentations;
4. **Plain:** fully expressive and unconstrained, without  $SO(3)$  equivariance.

In terms of geometric (*i.e.* function-fitting) expressivity, Models 3 and 4 are most expressive, while Model 1 is the most constrained. Model 2 leverages geometric structure for richer representations despite (intermediate) constraints.

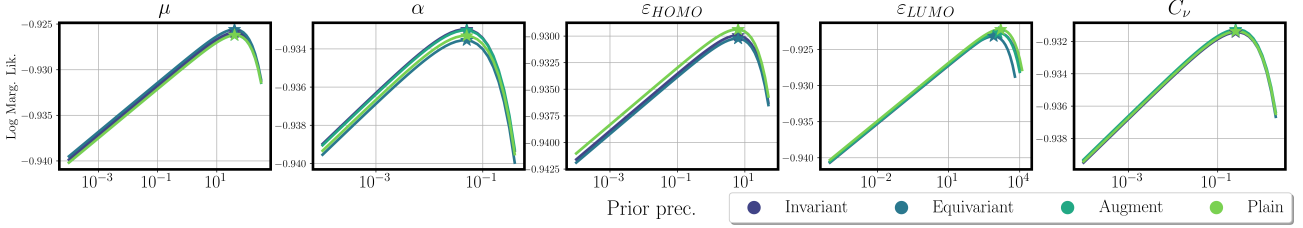


Figure 2: We optimize the Laplace approximation’s prior precision parameter  $\delta$  in a *post-hoc* fashion via grid search using the marginal likelihood (Eq. 5). We visualize the grid’s values and optimum (★) for every QM9 regression target and model.

**ModelNet40 classification results.** We visualize our results across various uncertainty-based measures in Fig. 1. Conformal and calibration measures closely align with prediction accuracy, and similarly suggest the unconstrained model (Plain) as the best fit for rotationally aligned data. In contrast, the Log-MargLik slightly favours the equivariant model despite its lower accuracy (*i.e.* presumed data fit), suggesting a slight effect of the model complexity term (discussed further in § 5). In contrast, for  $SO(3)$ -rotated ModelNet40 (Fig. 3) the geometric inductive bias becomes crucial, and all measures correctly identify the equivariant model as the preferred choice.

**QM9 regression results.** Tab. 1 reports results for prediction error – as measured via the *mean absolute error* or MAE – and the marginal likelihood (Log-MargLik), including its individual terms on data fit (LogLik) and model complexity (Eq. 5). Note that the Log-MargLik is rightly evaluated on the train data on which the Laplace approximation is computed. Measures on test data (incl. the Laplace’s test log-likelihood) clearly express a preferred model ranking in line with expectations on this  $SO(3)$ -affected task, that is Equivariant > Invariant > Augment > Plain. Conformal results are given in Fig. 4 and also align with the MAE. In contrast, the Log-MargLik fails to capture this trend and varies preferences across targets. Despite slight variations in train MAE the log-likelihoods are extremely similar and entirely dominate the complexity term, resulting in indistinguishable marginal likelihoods. Given the lack of coherence in obtained model complexities, we hypothesize that the objective thus fails to properly account for *geometric* expressivity or complexity as purportedly captured in the model’s feature structures. We discuss this effect next.

## 5 DISCUSSION & OUTLOOK

The marginal likelihood can also be leveraged in an “empirical Bayes” fashion to (even *post-hoc*) optimize hyperparameters of the Laplace approximation, such as the prior precision  $\delta$  [Immer et al., 2021]. Relating this step to a model’s feature expressivity, one might expect the prior precision of a more expressive model to be tuned higher as an intrinsic guard against data *over-fit* [Bishop, 2006], and

result in a larger complexity term in Eq. 5<sup>3</sup>. Nevertheless, our investigation on this relation in Fig. 2 finds the optimal value to be almost identical across all models. We interpret this as further evidence for our hypothesis that the feature differences induced by geometric constraints are not appropriately reflected in the marginal likelihood objective. Such geometry-induced structural differences clearly exist, as exemplified by Moskalev et al. [2023] (cf. their Fig. 2) who demonstrate that data-augmented models map transformed inputs to close but distinct locations in the representation space of last-layer activations, whereas strict invariance ensures a mapping to a single representation by design.

**Perspectives on a Geometric Occam’s Razor.** How to appropriately integrate geometric inductive biases into such a Bayesian framework in general fashion remains a seemingly open challenge. Several recent works have blended the two by framing geometric constraints as *learnable* parameters under a marginal likelihood objective. While promising, these approaches remain restricted in their generality to particular transformations (*e.g.*, the required degree of augmentation [Immer et al., 2022]) or model structures (*e.g.*, formulated as a Gaussian Process kernel [van der Wilk et al., 2018, Schwöbel et al., 2022]). Perhaps more generally, the integration of such constraints as regularizers with a possible Bayesian prior interpretation [Finzi et al., 2021, Kim et al., 2023a] or more explicit distributional correspondences [Bloem-Reddy et al., 2020, Kim et al., 2023b] could prove fruitful. We touch upon other related works in Appendix A.

**Conclusion.** We explore the use of *post-hoc* uncertainty-based measures to guide model selection among pretrained equivariant architectures. Conformal and calibration measures, while well aligned with predictive performance, offer limited insights into the underlying model fit. Bayesian model selection via the marginal likelihood shows partial promise, but fails to account for the differences in expressivity induced by geometric constraints. This seemingly points towards a mismatch between Bayesian and geometric notions of model complexity. Future work should strive towards integrating priors informed by equivariant representations to enable symmetry-aware Bayesian model selection.

<sup>3</sup>Albeit such trends implicitly assume that additional expressivity is not fully absorbed in the data fit term.

## References

- Anastasios N Angelopoulos, Stephen Bates, et al. Conformal prediction: A gentle introduction. *Foundations and Trends in Machine Learning*, 2023.
- Kenneth Atz, Francesca Grisoni, and Gisbert Schneider. Geometric deep learning on molecular representations. *Nature Machine Intelligence*, 2021.
- Simon Batzner, Albert Musaelian, Lixin Sun, Mario Geiger, Jonathan P Mailoa, Mordechai Kornbluth, Nicola Molinari, Tess E Smidt, and Boris Kozinsky. E(3)-equivariant graph neural networks for data-efficient and accurate interatomic potentials. *Nature Communications*, 2022.
- Edmon Begoli, Tanmoy Bhattacharya, and Dimitri Kusnezov. The need for uncertainty quantification in machine-assisted medical decision making. *Nature Machine Intelligence*, 2019.
- Erik J Bekkers, Sharvaree Vadgama, Rob Hesselink, Putri A Van der Linden, and David W Romero. Fast, expressive se(n)-equivariant networks through weight-sharing in position-orientation space. *International Conference on Learning Representations*, 2024.
- Christopher M Bishop. *Pattern recognition and machine learning*. Springer, 2006.
- Benjamin Bloem-Reddy, Yee Whye, et al. Probabilistic symmetries and invariant neural networks. *Journal of Machine Learning Research*, 2020.
- Johannes Brandstetter, Rob Hesselink, Elise van der Pol, Erik J Bekkers, and Max Welling. Geometric and physical quantities improve e (3) equivariant message passing. *International Conference on Learning Representations*, 2021.
- Glenn W Brier. Verification of forecasts expressed in terms of probability. *Monthly Weather Review*, 1950.
- Michael M Bronstein, Joan Bruna, Taco Cohen, and Petar Veličković. Geometric deep learning: Grids, groups, graphs, geodesics, and gauges. *arXiv Preprint (arXiv:2104.13478)*, 2021.
- Lung-Yi Chen and Yi-Pei Li. Uncertainty quantification with graph neural networks for efficient molecular design. *Nature Communications*, 2025.
- Taco Cohen and Max Welling. Group equivariant convolutional networks. *International Conference on Machine Learning*, 2016.
- Tiago Cortinhal, George Tzelepis, and Eren Erdal Aksoy. Salsanext: Fast, uncertainty-aware semantic segmentation of lidar point clouds. *Advances in Visual Computing*, 2020.
- Erik Daxberger, Agustinus Kristiadi, Alexander Immer, Runa Eschenhagen, Matthias Bauer, and Philipp Hennig. Laplace redux-effortless bayesian deep learning. *Advances in Neural Information Processing Systems*, 2021.
- Victor Dheur and Souhaib Ben Taieb. A large-scale study of probabilistic calibration in neural network regression. *International Conference on Machine Learning*, 2023.
- Marc Finzi, Gregory Benton, and Andrew G Wilson. Residual pathway priors for soft equivariance constraints. *Advances in Neural Information Processing Systems*, 2021.
- Matteo Fontana, Gianluca Zeni, and Simone Vantini. Conformal prediction: A unified review of theory and new challenges. *Bernoulli*, 2023.
- Huazhu Fu, Yitian Zhao, Pew-Thian Yap, Carola-Bibiane Schönlieb, and Alejandro F Frangi. Guest editorial special issue on geometric deep learning in medical imaging. *IEEE Transactions on Medical Imaging*, 2023.
- Jakob Gawlikowski, Cedrique Rovile Njiteucheu Tassi, Mohsin Ali, Jongseok Lee, Matthias Humt, Jianxiang Feng, Anna Kruspe, Rudolph Triebel, Peter Jung, Ribana Roscher, et al. A survey of uncertainty in deep neural networks. *Artificial Intelligence Review*, 2023.
- Pascal Germain, Francis Bach, Alexandre Lacoste, and Simon Lacoste-Julien. Pac-bayesian theory meets bayesian inference. *Advances in Neural Information Processing Systems*, 2016.
- Tilmann Gneiting, Fadoua Balabdaoui, and Adrian E Raftery. Probabilistic forecasts, calibration and sharpness. *Journal of the Royal Statistical Society Series B: Statistical Methodology*, 2007.
- Chuan Guo, Geoff Pleiss, Yu Sun, and Kilian Q Weinberger. On calibration of modern neural networks. *International Conference on Machine Learning*, 2017.
- Alexander Immer, Matthias Bauer, Vincent Fortuin, Gunnar Rätsch, and Khan Mohammad Emtiyaz. Scalable marginal likelihood estimation for model selection in deep learning. *International Conference on Machine Learning*, 2021.
- Alexander Immer, Tycho van der Ouderaa, Gunnar Rätsch, Vincent Fortuin, and Mark van der Wilk. Invariance learning in deep neural networks with differentiable laplace approximations. *Advances in Neural Information Processing Systems*, 2022.
- Ramneet Kaur, Susmit Jha, Anirban Roy, Sangdon Park, Edgar Dobriban, Oleg Sokolsky, and Insup Lee. iDECODE: In-distribution equivariance for conformal out-of-distribution detection. *AAAI Conference on Artificial Intelligence*, 2022.

- Hyunsu Kim, Hyungi Lee, Hongseok Yang, and Juho Lee. Regularizing towards soft equivariance under mixed symmetries. *International Conference on Machine Learning*, 2023a.
- Jinwoo Kim, Dat Nguyen, Ayhan Suleymanzade, Hyeokjun An, and Seunghoon Hong. Learning probabilistic symmetrization for architecture agnostic equivariance. *Advances in Neural Information Processing Systems*, 2023b.
- Benjamin Kompa, Jasper Snoek, and Andrew L Beam. Empirical frequentist coverage of deep learning uncertainty quantification procedures. *Entropy*, 2021.
- Volodymyr Kuleshov, Nathan Fenner, and Stefano Ermon. Accurate uncertainties for deep learning using calibrated regression. *International Conference on Machine Learning*, 2018.
- George Lamb and Brooks Paige. Bayesian graph neural networks for molecular property prediction. *NeurIPS Workshop on Machine Learning for Molecules*, 2020.
- Jing Lei, Max G’Sell, Alessandro Rinaldo, Ryan J Tibshirani, and Larry Wasserman. Distribution-free predictive inference for regression. *Journal of the American Statistical Association*, 2018.
- Fernando Llorente, Luca Martino, David Delgado, and Javier Lopez-Santiago. Marginal likelihood computation for model selection and hypothesis testing: an extensive review. *SIAM Review*, 2023.
- Sanae Lotfi, Pavel Izmailov, Gregory Benton, Micah Goldblum, and Andrew Gordon Wilson. Bayesian model selection, the marginal likelihood, and generalization. *International Conference on Machine Learning*, 2022.
- Clare Lyle, Mark van der Wilk, Marta Kwiatkowska, Yarin Gal, and Benjamin Bloem-Reddy. On the benefits of invariance in neural networks. *arXiv Preprint (arXiv:2005.00178)*, 2020.
- David JC MacKay. A practical bayesian framework for backpropagation networks. *Neural Computation*, 1992.
- David JC MacKay. *Information theory, inference and learning algorithms*. Cambridge University Press, 2003.
- Spyros Makridakis and Nikolas Bakas. Forecasting and uncertainty: A survey. *Risk and Decision Analysis*, 2016.
- Lewis H Mervin, Simon Johansson, Elizaveta Semenova, Kathryn A Giblin, and Ola Engkvist. Uncertainty quantification in drug design. *Drug Discovery Today*, 2021.
- Artem Moskalev, Anna Sepliarskaia, Erik J Bekkers, and Arnold WM Smeulders. On genuine invariance learning without weight-tying. *ICML Workshop on Topological, Algebraic and Geometric Learning*, 2023.
- Allan H Murphy. A new vector partition of the probability score. *Journal of Applied Meteorology and Climatology*, 1973.
- Jeremy Nixon, Michael W Dusenberry, Linchuan Zhang, Ghassen Jerfel, and Dustin Tran. Measuring calibration in deep learning. *CVPR Workshop*, 2019.
- Mircea Petrache and Shubhendu Trivedi. Approximation-generalization trade-offs under (approximate) group equivariance. *Advances in Neural Information Processing Systems*, 2023.
- Christina Petschnigg, Markus Spitzner, Lucas Weitzendorf, and Jürgen Pilz. From a point cloud to a simulation model—bayesian segmentation and entropy based uncertainty estimation for 3d modelling. *Entropy*, 2021.
- Raghunathan Ramakrishnan, Pavlo O Dral, Matthias Rupp, and O Anatole Von Lilienfeld. Quantum chemistry structures and properties of 134 kilo molecules. *Scientific Data*, 2014.
- Carl Rasmussen and Zoubin Ghahramani. Occam’s razor. *Advances in Neural Information Processing Systems*, 2000.
- David W Romero and Suhas Lohit. Learning partial equivariances from data. *Advances in Neural Information Processing Systems*, 2022.
- Mauricio Sadinle, Jing Lei, and Larry Wasserman. Least ambiguous set-valued classifiers with bounded error levels. *Journal of the American Statistical Association*, 2019.
- Pola Schwöbel, Martin Jørgensen, Sebastian W Ober, and Mark Van Der Wilk. Last layer marginal likelihood for invariance learning. *International Conference on Artificial Intelligence and Statistics*, 2022.
- Glenn Shafer and Vladimir Vovk. A tutorial on conformal prediction. *Journal of Machine Learning Research*, 2008.
- Telmo Silva Filho, Hao Song, Miquel Perello-Nieto, Raul Santos-Rodriguez, Meelis Kull, and Peter Flach. Classifier calibration: a survey on how to assess and improve predicted class probabilities. *Machine Learning*, 2023.
- Ava P Soleimany, Alexander Amini, Samuel Goldman, Daniela Rus, Sangeeta N Bhatia, and Connor W Coley. Evidential deep learning for guided molecular property prediction and discovery. *ACS Central Science*, 2021.
- Sharvaree Vadgama, Mohammad Mohaiminul Islam, Domas Buracus, Christian Shewmake, and Erik Bekkers. On the utility of equivariance and symmetry breaking in deep learning architectures on point clouds. *arXiv Preprint (arXiv:2501.01999)*, 2025.

Putri A. van der Linden, Alejandro García-Castellanos, Sharvaree Vadgama, Thijs Kuipers, and Erik J. Bekkers. Learning symmetries via weight-sharing with doubly stochastic tensors. *Advances in Neural Information Processing Systems*, 2024.

Putri A. van der Linden, Alexander Timans, and Erik J. Bekkers. CP<sup>2</sup>: Leveraging Geometry for Conformal Prediction via Canonicalization. *Conference on Uncertainty in Artificial Intelligence*, 2025.

Tycho van der Ouderaa, Alexander Immer, and Mark van der Wilk. Learning layer-wise equivariances automatically using gradients. *Advances in Neural Information Processing Systems*, 2023.

Mark van der Wilk, Matthias Bauer, ST John, and James Hensman. Learning invariances using the marginal likelihood. *Advances in Neural Information Processing Systems*, 2018.

Maurice Weiler and Gabriele Cesa. General  $e(2)$ -equivariant steerable cnns. *Advances in Neural Information Processing Systems*, 2019.

Tom Wollschläger, Nicholas Gao, Bertrand Charpentier, Mohamed Amine Ketata, and Stephan Günnemann. Uncertainty estimation for molecules: Desiderata and methods. *International Conference on Machine Learning*, 2023.

Zhirong Wu, Shuran Song, Aditya Khosla, Fisher Yu, Linguang Zhang, Xiaoou Tang, and Jianxiong Xiao. 3d shapenets: A deep representation for volumetric shapes. *Conference on Computer Vision and Pattern Recognition*, 2015.

# On Equivariant Model Selection through the Lens of Uncertainty

## — Supplementary Material —

### A OTHER RELATED WORK

Bayesian (and other) approaches to uncertainty quantification have been recently applied to molecular point cloud data, often using domain-specific desiderata to assess reliability [Lamb and Paige, 2020, Soleimany et al., 2021, Wollschläger et al., 2023], as well as in molecule and drug design [Mervin et al., 2021, Chen and Li, 2025]. In 3D vision, uncertainty methods have been applied to more general point cloud segmentation and classification [Petschnigg et al., 2021, Cortinhal et al., 2020]. Finally, several works leverage geometry or equivariance properties to inform conformal procedures [Kaur et al., 2022, van der Linden et al., 2025]. These approaches leverage uncertainty primarily for predictive purposes, not for general model selection.

### B IMPLEMENTATION DETAILS

Model	Parameter counts			
	ModelNet40		QM9	
	Feature extractor	Last layer	Feature extractor	Last layer
Invariant	1.664.896		4.638.208	
Equivariant	1.994.752	5160	5.131.904	257
Augment	1.669.504		4.642.816	
Plain	1.669.504		4.642.816	

Table 2: Model sizes for the feature extractors and their last layers. All models share the same penultimate feature dimension within each dataset, and hence have the same last layer size.

**Parameter counts.** Tab. 2 shows model sizes in terms of parameter counts for all models. All models except **Plain** are trained with  $SO(3)$  data augmentation. For both ModelNet40 and QM9 we follow the architecture-specific hyperparameter configurations described in Vadgama et al. [2025].

**ModelNet40 training.** Models are trained for 250 epochs with a final layer dimension of 128. We use a 7375/2468/2468 train/validation/test split, sampling 1024 points per object. All point clouds are spatially centered and normalized, and training samples are further augmented with small random shifts drawn from  $\mathcal{U}([0.0, 0.1])$ .

**QM9 training.** Models are trained for 300 epochs with a final layer dimension of 256. During training, node coordinates are normalized using a global scale and shift computed from the training set. We use a 110000/10000/10831 train/validation/test split.

**Conformal prediction sets.** In both experiments we consider standard split conformal prediction leveraging a hold-out calibration set for the conformal procedure, and evaluating on test data [Angelopoulos et al., 2023]. We additionally repeat 100 random resamples of calibration and test data splits for the mean prediction set sizes (for classification) and interval widths (for regression) following Eq. 4. We set the target coverage level to  $(1 - \alpha) = 0.9$ , *i.e.* a desired coverage rate of 90%. We omit reporting coverage since the rate is equally satisfied across all models (by design). For classification we use a simple thresholding nonconformity score which ranks predictions based on the model’s confidence in the true class label [Sadinle et al., 2019]. For regression we adopt the absolute residual between predicted and true target as a simple nonconformity score [Lei et al., 2018].

## C ADDITIONAL EXPERIMENTAL RESULTS

**Rotated ModelNet40 classification results.** Our experimental design for ModelNet40 is additionally employed for the rotated data setting, wherein train, validation, and test data are randomly transformed by elements from the  $SO(3)$  group. Results are shown in Fig. 3. We omit the unconstrained model (**Plain**) as it performs extremely poorly due to lack of  $SO(3)$  generalization and is therefore uninformative. Results for the other methods highlight the same alignment observed in Fig. 1.

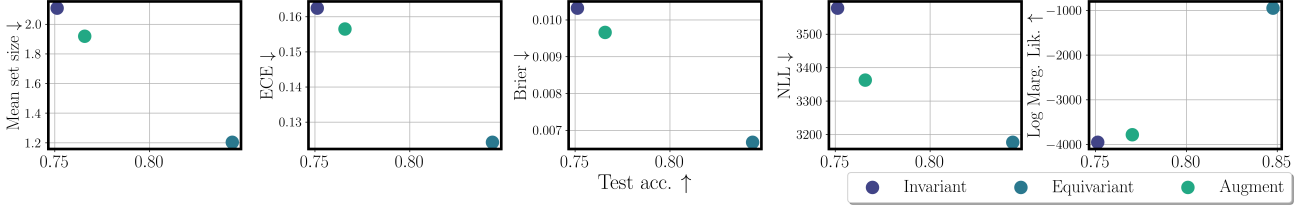


Figure 3: We visualize alignment between uncertainty-based measures ( $y$ -axis) and prediction accuracy ( $x$ -axis) on **rotated** ModelNet40 test data for three models. ‘NLL’ refers to the *negative log-likelihood* of the model’s direct softmax output (*i.e.* not using Laplace), while ‘Log Marg Lik’ equates Eq. 5. ( $\uparrow\downarrow$ ) indicate the desired direction of the measure.

**Conformal prediction set size for QM9 regression.** We display the conformal mean set size (*i.e.* interval widths) for considered QM9 regression targets in Fig. 4. Consistent with the trends discussed in § 4 and Fig. 3 the measure closely aligns with predictive performance.

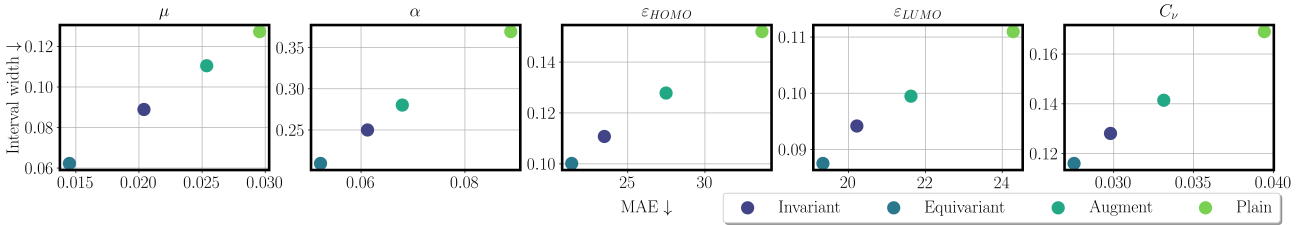


Figure 4: We visualize alignment between conformal mean set sizes or interval widths ( $y$ -axis) and prediction error ( $x$ -axis) for all four models (§ 4) and five regression targets on QM9. ( $\uparrow\downarrow$ ) indicate the desired direction of the measure.